OPERATIONS AT THE JPL OCTL TELESCOPE

Keith E. Wilson- Keith.E.Wilson@jpl.nasa.gov, Joseph Kovalik-Joseph.M.Kovalik@jpl.nasa.gov,
Abhijit Biswas- Abhijit.Biswas@jpl.nasa.gov,
William T. Roberts-William.T.Roberts@jpl.nasa.gov
Jet Propulsion Laboratory
MS 161-135, 4800 Oak Grove Dr.
Pasadena, CA 91109

ABSTRACT

The JPL Optical Communications Telescope Laboratory (OCTL) is a 200 sq-m located at 2.2.km altitude in Wrightwood California and houses a state-of-the-art 1-m telescope. The OCTL team is involved in the development of operational strategies for ground-to-space laser beam propagation for future NASA optical communications missions. Strategies include safe beam propagation through navigable air space, line of sight optical attenuation monitoring, adaptive optics, and multi-beam scintillation mitigation. This paper presents the results of recent operations at the OCTL facility including telescope characterization data and laser beam propagation experiments to Earth-orbiting retro-reflecting satellites; experiments that validate the telescope's tracking and blind-pointing performance and safe laser beam transmission procedures for propagating through navigable airspace.
Key words: Optical communications, lasers, safe laser beam propagation, uplink scintillation mitigation.

1. INTRODUCTION

It is well recognized that optical communications offers higher bandwidth communications in smaller, lower mass, and less power-consuming spacecraft subsystems [1]. Such high bandwidth links are an enabling communications technology for missions flying high data rate high-resolution instruments. A technology under development, the operational issues associated with optical communications are still being explored, and strategies to mitigate atmospheric effects are being developed [2,3,4].

The JPL Optical Communications Telescope Laboratory (OCTL) shown in Figure 1 is an R&D facility designed to investigate and address issues that affect ground-to-space optical communications to NASA's near-Earth and deep space probes. Located at 34° 22.9' North Latitude, 117° 40.9' West Longitude and 2.2 km altitude in the San Gabriel mountain range of Southern California, the OCTL facility lies above the densest part of the atmosphere where atmospheric seeing typically ranges from 0.5 to 2 arc secs at night and 2 to 5 arc secs during the day.

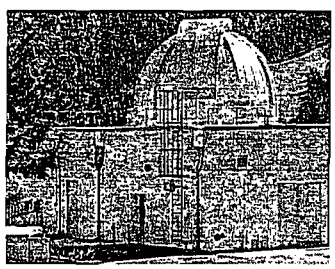

Figure 1: OCTL building is located at 7400-ft elevation on JPL's Table Mountain Facility. It houses a 1-m coudé focus satellite-tracking telescope.

OCTL's telescope is a 1-m, f/75.8 a coudé focus instrument that can be rapidly accessed from any one of four ports to support high power laser beam propagation and reception. A 20-cm acquisition telescope bore sighted to the main telescope allows bi-static operation with transmission and/reception from either or both telescope apertures. In addition, this smaller telescope is used as the receiver for line-of-sight cloud detection. Designed to support satellite tracking from low-Earth orbit to deep space, the telescope slews at speeds up to 10 deg/sec in elevation and 20 deg/sec in azimuth. Built to support both daytime and nighttime operation the primary mirror is enclosed in louvered baffles to allow pointing as close as 10 degrees of the sun.

In this paper we describe results of recent operations at the OCTL telescope. In Section 2 we present the results of telescope blind pointing and tracking tests and in Section 3 we present the initial results from satellite tracks with narrow laser beams. In Section 4 we describe a three-tiered system for safe laser beam propagation through near-Earth and navigable air space.

2. OCTL TRACKING AND BLIND POINTING

The blind pointing performance of the telescope is essential to the initial acquisition or re-acquisition. For optical communications the blind pointing accuracy will determine the divergence and scan strategy of the uplink beam from the ground to initiate the link with the target spacecraft. Measurements were made under a variety of atmospheric conditions, and our initial results show a correlation with the variance in wind speed. Two approaches were used to make blind pointing and tracking measurements. In the first technique, the output telescope's coudé focus video camera was displayed on a calibrated monitor and blind pointing and tracking drift measurements were made relative to the central cross hairs. The second technique was used for later measurements and allowed atmospheric seeing to be recorded concurrently with the telescope's blind pointing and tracking measurements. Here, the star images were made incident on a 4Kx4K pixel science camera. The camera exposure was typically five seconds with measurements made at five-minute intervals.

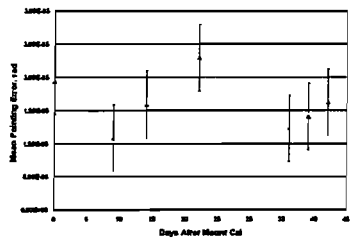

Figure 2: Mean blind pointing error as a function of days after telescope mount calibration.

Figure 2 plots blind-pointing error as a function of days after mount calibration. The data show no dependence of the blind pointing error on the age of the mount calibration out to forty-five days after calibration. With optimum mount calibration the blind-pointing error is affected by temperature and by the buffeting of the telescope structure by wind. The measured tracking performance is affected and by both lower winds and the upper atmospheric winds that affect "seeing" and hence the motion of the image in the focal plane. The tracking drift rate and the blind pointing error were measured at random intervals over six-month period. The results are shown in Figures 3 and 4. The mean pointing error over the six-month test period was 19.9μrad±7.5μrad, the average tracking drift rate shown in Figure 4 was 11.7 μrad/hr±6 μrad/hr, which is comparable to the atmospheric seeing. These data were taken under a variety of wind conditions; in particular the data point of 27-μrad/hr tracking drift in Figure 4 corresponds to April 19, 2007 under sustained winds of 18 km/hr with gusts up to 30 km//hr at the facility.

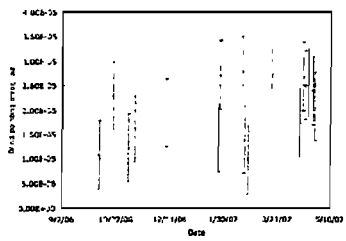

Figure 3: Telescope blind pointing error measured over six-month period from October 2006 to April 2007 The measurements were made under a variety of wind and temperature conditions. The mean error is 19.9μrad±7.5μrad.

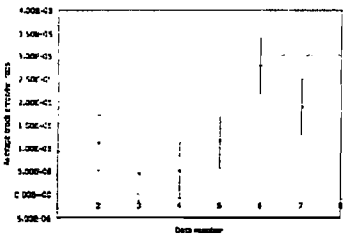

Figure 4:Average telescope drift per hour when pointed to a star. Measurements were made under a variety of wind loading conditions.

Figure 5 is a measurement of the atmospheric seeing over a ninety-minute period the night of May 8, 2007made using the second approach. The mean atmospheric seeing was 1.5 arc-sec (7.5 μrad) ±0.5 arc-sec. The mean temperature was 12°C, relative humidity 17% and mean wind speed 1.6km/hr with gusts to 3.2 km/hr. Figure 6 gives the telescope's tracking performance over the same time period. The 1σ drift rate over the period was 3.6-μrad/hr.

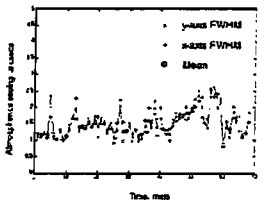

Figure 5: Atmospheric seeing measured on the night of May 8, 2007 at the OCTL.

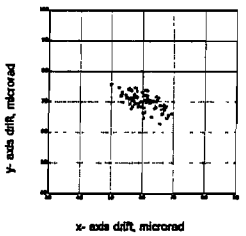

Figure 6: Tracking drift shown over a ninety-minute period on May 8, 2007.

3. ACTIVE SATELLITE TRACKING

In contrast to operations at laser tracking stations, where uplink beams are on the order of 0.1mrad to 1-mrad, the objective of the OCTL satellite tracking experiments is to develop strategies for pointing narrow laser beams (.02mrad - 0.03mrad) to deep space probes. JPL has received permission from satellite owners to illuminate more than twenty retro-reflecting satellites. To date, we have successfully transmitted to EGP-1, Stella, Starlette, and Beacon C; satellites for which CPF files are available [5]. The return signal from retro-reflector bearing satellite can be estimated using the radar link equation (1) below:

$$S = E_p\left(\frac{\lambda}{hc}\right)\eta_{TX}G_T L_P L_s \sigma_{BS}\eta_{atm}^2 L_{atm_Spread} L_{atm_point} A\eta_{Rx_Tel}\eta_{Strehl}\eta_{opt_train}\eta_{POL} \qquad (1)$$

A flashlamp-pumped laser operating at 50 Hz was used as the uplink. The laser has two Nd:YAG rods in an unstable Gaussian-coupled resonator cavity that allows for efficient energy extraction. In the Q-switched mode it emits 600-mJ, 8-ns pulses at the 1064-nm fundamental frequency. At the Type-II KTP frequency-doubled output the laser emits a 250-mJ, 8-ns long pulse. To avoid pulse collision from more distant target satellites, the laser is operated at sub-multiples of the lamp pulse repetition rate (PRF). It emits a 7.4 mm x 11.5 mm elliptical beam with divergence of approximately 0.5-milliradian at 532-nm, and 1.9-milliradians at 1064-nm. To maintain the thermal loading in the cavity constant with changes in PRF, the flashlamp PRF is maintained at 50-Hz while the Q-switch repetition rate is changed. This maintained a constant beam divergence for the different repetition rates, eliminating the need to realign the optical train for different ranges of the target satellites.

In these early experiments, satellites were tracked primarily during terminator passes to visually confirm the telescope acquisition and tracking. Figure 7 is a comparison of link analysis prediction to experimental results for the October 23 Ajisai pass. The full angle uplink beam divergence was 30-μrad full angle. The fit to the data assumed a 3σ pointing error of 15-μrad. There were no clouds visible at the time of the pass, and winds speeds ranged between 1.6-km/hr and 3.2-km/hr. The large variation in signal return strength observed during the pass is probably due to fluctuations in beam jitter, tracking errors, and uplink beam scintillation.

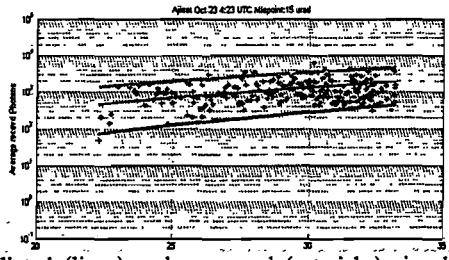

Figure 7: Comparison of predicted (lines) and measured (asterisks) signal returns expressed as number of incident photons versus elevation angle of spacecraft. The 532-nm laser was transmitted from OCTL in the mono-static configuration.

LASER BEAM PROPAGATION SYSTEM

Figure 8 is a schematic of the AST beam delivery system. The Spectra Physics BeamLok laser beam pointing stabilization system is integrated with the laser to maintain an output beam pointing stability of 25-μrad. The half wave plates before the Brewster prism polarizer adjusted the polarization so that there was equal power in the reflected and transmitted beams. The half wave plate after the polarizer reoriented the polarization of the transmitted beam so that it was parallel to that of the reflected beam. The beams were reflected by a series of mirrors to the beam control lens that set the laser focus at the location in the beam path to obtain the required beam size in the telescope pupil.

The design of the beam delivery system was constrained by (i) damage to the M7 mirror and (ii) the need to maintain the

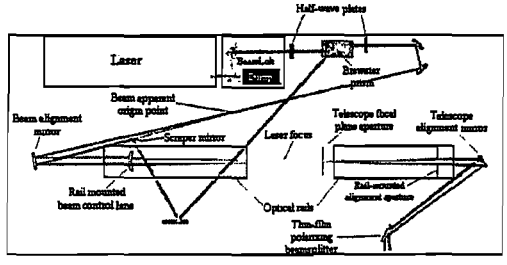

spot size on the telescope pupil to less than 30-cm to minimize vignetting the beam. The nominal focus of the f/75.8 telescope was approximately 2-m from the M7 mirror. Because the power density of the beam at the M7 was 1.2-J/cm^2 and exceeded the damage threshold of the mirror, the telescope focus was extended beyond its nominal position and we used a dual beam uplink that also served to mitigate the effects of uplink scintillation. This resulted in a factor of eight reduction in the power density on the M7 mirror

Figure 8: Layout of active satellite tracking optical train.

The basic configuration was a mono-static design with the uplink transmitted through two sub-apertures on the telescope primary. The full 1-m aperture was used for reception. The detectors were Hamamatsu photomultipliers (PMT); the H5783-20 for 532-nm operation and the Hamamatsu 9170 NIR for 1064-nm operation. For terminator passes, light from sunlit spacecraft along with retro-reflected laser signals were transmitted through the telescope; a portion of the randomly polarized light was made incident on the thin-film polarizing beam splitter shown in Figure 8. P-polarized light transmitted through the beam splitter was reflected from a broadband silver-coated flat mirror (not shown), toward the optical receiver box that protected the PMT from stray light. Dichroic beam splitters reflected the signal wavelength (532-nm or 1064-nm) onto the PMT, while the light from the sunlit satellites was transmitted and focused onto a CCD camera.

In the bi-static configuration, the 20-cm F/7.5 Newtonian acquisition telescope bore-sighted with the main telescope served as the receiver. Approximately 50 meters of 200-μm core optical fiber including service loops guided the light from the

telescope focus to the PMT. The advantage of this approach was that it provided excellent transmit/receive isolation, protecting the sensitive detectors from backscatter off the optical surfaces in the transmitter optical train. The disadvantage was a 7-dB signal loss due to the smaller aperture.

DATA ACQUISITION SYSTEM

The data acquisition system used a personal computer running windows software and a commercial-off-the-shelf single-channel digitizer card by Signatec with a bandwidth of 500-MHz at a sampling rate up to 1 Gigasample/second (Gs/s). The control and analysis software was written in National Instrument's LabVIEW programming environment to create virtual instruments that both display data in real time and give the user interactive control through a graphical user interface. The software generated satellite state vector files to point the telescope.

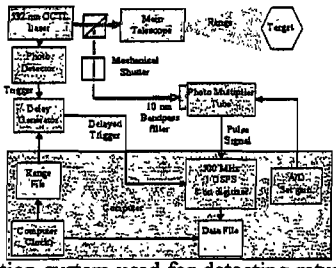

Figure 9: Block diagram of the data acquisition system used for detecting returns from the OCTL 532-nm laser. The mechanical shutter in front of the PMT is driven by the laser Q switch and is closed for a period of time immediately after the laser fires. This prevents any Rayleigh backscatter from the atmosphere or any stray scatter from the laser room itself entering the PMT.

A block diagram of the data acquisition system for detecting return pulses from the OCTL 532-nm laser is shown in Figure 9. The LabVIEW VI shown in Figure 10 controls the Signatec model PDA100 PCI waveform digitizer card and the Stanford Research systems (SRS) DG 535 delay generator via a National Instruments model NI-488.2 USB to GPIB interface. The PMT gain was set with a control voltage determined in the VI by the user and generated by a National Instruments model USB-6008 digital to analog converter. The digitizer has an onboard memory of 4 Mega samples corresponding to a range window of 600-km for a 1 nanosecond (ns) sampling time. The ranges to the target satellites varied from a few hundred to a few thousand kilometers over a given pass. Direct triggering of the digitizer by the outgoing laser pulse would not provide a long enough time window in which to acquire the retro-reflected pulse. The outgoing pulse trigger was thus delayed by a time interval corresponding to the round trip time of flight to the satellite, less half of the range window of up to 100-km after which time it triggered the digitizer. The return pulse then fell in the center of the range window. The range window was limited to 100-km due to memory constraints of the computer.

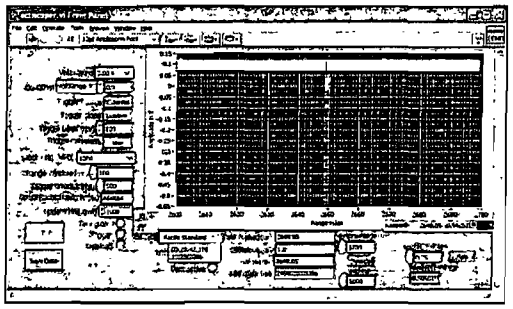

Figure 10: LabVIEW VI user interface for viewing and recording data

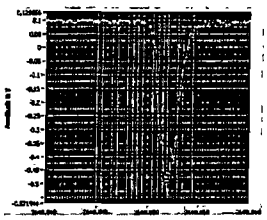

Figure 11: Return pulse from an Ajisai pass at 10:29:42 UTC on October 20, 2006 when the satellite had an expected range of 2649.05-km.

(a) (b)

Figure 12: (a) Plot of measured range and expected range over an Ajisai satellite pass. (b) Plot of the difference of the expected range from the measured range. The difference is also plotted with the computer clock offset by a constant 0.434 seconds to account for a lack of synchronization between the computer clock and the GPS clock.

The CPF file with the range of the satellite as a function of time was loaded into the data acquisition program at the inception. The VI used the internal clock of the computer as a time reference from which to interpolate the instantaneous range of the. A photo detector on the optics bench detected the output laser pulses and was used to trigger the DG535. The delayed trigger from the DG535 then triggered the digitizer. These data were time-tagged, displayed and saved along with the time-tagged return signal detected by the PMT for post-processing. Figure 11 shows a return pulse taken from an Ajisai pass at 10:29:42 UTC on October 20, 2006. The output was the 532-nm frequency-doubled Nd:YAG laser output with a pulse width of about 8-ns.

The position of the pulse peak was used to determine the actual arrival time of the return signal. A plot of the measured range as a function of time can be seen in Figure 12 (a). Figure 12 (b) shows the difference of the expected range from the measured range. The difference is also plotted with a constant offset applied to the measured arrival time to correct for the synchronization error between the computer's clock that determined by a GPS clock.

4. LASER SAFETY SYSTEM

The OCTL laser safety system starts with safe laser beam operation inside the laboratory. JPL's safety requirements stipulate that (i) all persons present in the coudé room during laser operation be certified to have completed a JPL-approved laser safety training course, (ii) the appropriate eye protection equipment be used by persons present in the coudé room during operation, (iii) door interlocks are to be activated to avoid inadvertent entry to the coudé room when the laser is operating. In addition, safety signs specifying the wavelengths and output powers of the lasers in the facility are posted at the entry doors to the coudé room and lighted notifications of laser operation are located both at the entrance to the facility and the coudé room.

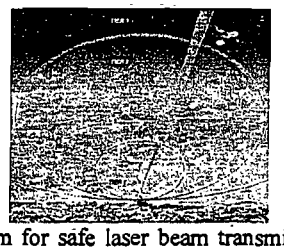

Figure 13: Three-tiered outdoor laser safety system for safe laser beam transmission through navigable air space and the near-Earth space environment.

For laser propagation out of the facility, JPL has coordinated with the FAA and the Laser Clearinghouse to ensure safe laser beam propagation through navigable air space and through the near-Earth space environment. Figure 13 shows the JPL-developed three-tiered laser safety system. Tiers -1 and 2 are within navigable airspace and sensors detect aircraft at risk of entering the laser beam. Tier-1 extends approximately 4-km from the facility and is monitored by wide field and narrow field long-wave infrared (LWIR) sensors. The Tier-1 ILI camera system is currently being evaluated as a possible substitute for the outside observer. Currently, it is supported by observers positioned around the facility to alert the safety system operator of aircraft at risk of intercepting the laser beam, a FAA requirement. The Tier-2 sensor is a Primus-40

weather radar bore-sighted to the telescope. The radar beam is emitted in 3-μsec long pulses at 121 Hz with peak power of 8-kW. To protect the sensitive receivers the Primus-40 radar system has approximately a 3-μsec blanking period when the receivers are turned off.

5. SUMMARY

We have described recent experiments conducted at the OCTL to characterize the telescope's blind pointing and tracking performance. Our results show that the telescope's mount calibration holds over several weeks and performance is most affected by wind gusts. Measurements made on a quiescent night in 1.5 arc-sec seeing conditions and 1.6-km/hr winds show tracking drifts of less than 4μrad/hr. We have successfully illuminated several target satellites with narrow (20μrad-30μrad) beams to validate the telescope's performance and to develop operational strategies for future deep space optical communications demonstrations. Future work calls for demonstrating high precision ranging with these narrow beams that are capable of supporting uplink optical communications to interplanetary probes.

6. ACKNOWLEDGEMENTS

The original research for this report was carried out by the Jet Propulsion Laboratory, California Institute of Technology, under contract with the National Aeronautics and Space Administration.

The authors would like to thank Drs. D. Antsos and F. Davarian for their continued programmatic support, Mr. A. Grigsby and Ms. D. Mayes of the OCTL team for their continued diligence and operations support, Dr. W. Owen for his support in preparing the CPF files for satellite tracking, and Dr. G. Ortiz for his assistance in reducing the more recent seeing and tracking data.

7. REFERENCES

1. H. Hemmati, K. Wilson, M. Sue, M. Wilhelm, D. Rascoe, F. Lansing, L. Harcke, and C. Chen, " Comparative Study of Optical and RF Communications Systems for a Mars Mission", SPIE Free-Space Laser Communications Technologies Proceedings, Jan. 1996, San Jose, CA.
2. Wilson, K. E., and J. R. Lesh, "An Overview of the Galileo Optical Experiment (GOPEX)," TDA PR 42-114, April-June 1993, pp. 192-204, August 15, 1993.
3. Wilson, K. E., "An Overview of the GOLD Experiment Between the ETS-VI Satellite and the Table Mountain Facility," TDA PR 42-124, October-December 1995, pp. 8-19, February 15, 1996.
4. K. Wilson, M. Wright, R. Cesarone, K. Shea, "Cost and Performance Comparison of an Earth-Orbiting Optical-comm Relay Transceiver and a Ground-based Optical Receiver Subnet", JPL TDA Progress Report 142-153, May 2003.
5. ftp://cddis.gsfc.nasa.gov/pub/slr/cpf_predicts